Dynamical, dielectric, and elastic properties of GeTe investigated with first-principles density functional theory

R. Shaltaf,[1,2] E. Durgun,[3,4] J.-Y. Raty,[5] Ph. Ghosez,[3,4] and X. Gonze[1,2]
[1]*European Theoretical Spectroscopy Facility (ETSF)*
[2]*Unité Physico-Chimie et de Physique des Matériaux, Université Catholique de Louvain, B-1348 Louvain-la-Neuve, Belgium*
[3]*European Multifunctional Materials Institute (EMMI)*
[4]*Physique Theorique des Matériaux, Université de Liège (B5), B-4000 Liège, Belgium*
[5]*FRS-FNRS, Département de Physique, Université de Liège (B5), B-4000 Liège, Belgium*
(Received 31 March 2008; published 14 November 2008)

The dynamical, dielectric, and elastic properties of GeTe, a ferroelectric material in its low-temperature rhombohedral phase, have been investigated using first-principles density functional theory. We report the electronic energy bands, phonon-dispersion curves, electronic and low-frequency dielectric tensors, infrared reflectivity, Born effective charges, and elastic and piezoelectric tensors and compare them with the existing theoretical and experimental results, as well as with similar quantities available for other ferroelectric materials, when appropriate.

DOI: 10.1103/PhysRevB.78.205203 PACS number(s): 77.84.−s, 77.22.−d, 62.20.D−, 77.65.−j

I. INTRODUCTION

GeTe is an interesting material from both academic and industrial perspectives. When alloyed with antimony, the electronic and optical properties of GeTe get dramatically modified due to the change in the microscopic structure from the crystalline to the amorphous phase.[1–3] This makes it a crucial base material in phase-change alloys used in optical storage rewritable compact disks (CDs) and digital versatile disks (DVDs).

Besides this technological interest, GeTe attracts more academic-oriented interest for its ferroelectric properties. At higher temperatures, it possesses the highly symmetric, paraelectric, and rocksalt cubic structure (space group $F3m$ No. 225). Below a critical temperature T_c, it stabilizes in a lower symmetry ferroelectric structure (space group $R3m$ No. 160) with Ge and Te ions being displaced from ideal rocksalt sites. The ferroelectric transition is characterized by the softening of a zone-center transverse optic (TO) phonon mode propagating in the [111] direction and the freezing in of a relative displacement of the crystal sublattices.[4] Unlike other IV-VI telluride-based materials, such as SnTe and PbTe which have very low T_c of ~ 140 K and less than 2 K, respectively, GeTe has $T_c \sim 720$ K, which makes it the simplest ferroelectric material existing at room temperature with only two atoms per primitive cell.

Due to its interesting properties as ferroelectric and phase-change material, GeTe has been the subject of many experimental and theoretical studies. The electronic, structural, and optical properties have been investigated in the different crystalline, liquid, or amorphous phases.[4–13] The cubic phase instability and pressure-induced phase transition have been the issue of discussion in some studies.[8–14] However the dynamical, mechanical, and piezoelectric properties of GeTe have been largely left aside.

A Raman inelastic-scattering study of GeTe was carried out in the early work of Steigmeier and Harbeke,[4] who found two principal peaks: a first peak at a frequency of 98 cm^{-1}, which is attributed to a degenerate E mode, and a second peak at 140 cm^{-1}, which is attributed to a A_1 mode. A more recent experimental study has reported values of 80 and 122 cm^{-1} for the E and A_1 modes, respectively.[5]

Calculations of dynamical properties of GeTe using density functional perturbation theory (DFPT) were reported by Zein *et al.*,[8] who studied the GeTe in the high-temperature rocksalt structure. They found soft phonon at Γ and reported a value of $\sim 10.2e$ for the Born effective charge. Dielectric properties of the rocksalt structure were also investigated by Waghmare *et al.*,[15] who reported the Born effective charge, the LO-TO splitting, and the optical dielectric constants. However, the dielectric properties of GeTe in the stable ferroelectric phase have not been examined. Ciucivara *et al.*[13] used *ab initio* calculations reporting a value of $10.11e$ for the Born effective charge in the ferroelectric phase. Whereas such a value is very close to the value previously reported for the rocksalt structure,[8] it is in clear contrast with the behavior for perovskites where large Born effective charge modifications due to the ferroelectric transition have been reported.[16]

The aim of our work is to perform a comprehensive study of the electronic, dynamical, dielectric, elastic, and piezoelectric properties of GeTe in its low-temperature rhombohedral phase. Doing so, we uncover some problems with previous calculations. The correct understanding of the bulk ferroelectric phase of GeTe is a prerequisite for future investigations of the ferroelectric properties of the more complex GeTe nanostructures.[17,18] Recent experimental results have shown that GeTe nanowires are very promising for scalable memory applications.[18] It has been shown also that zero-dimensional ferroelectrics can have a vortex structure for their dipoles below a critical temperature. The possibility of switching the direction of the toroidal moment can have many important applications in nanomemory devices, nanomotors, nanotransducers, nanoswitchers, nanosensors, etc.[19,20]

This paper is organized as follows. In Sec. II, we present the details of the methods used in the present study. In Sec. III, we discuss the ground-state structural and electronic

 ©2008 The American Physical Society

TABLE I. Calculated structural parameters of GeTe. The lattice parameter a_0 (in angstrom), the angle α (in degrees), the deviation of the Ge sublattice from the 0.5 sublattice position τ, and the volume $\Omega=(a_0^3/4)\sin^2\alpha$ (in Å^3). The calculated lattice constants a and c (in angstrom) of the equivalent hexagonal representation of the unit cell are also presented.

	a_0	α	τ	Ω	a	c
Present	5.893	88.96	0.0236	51.15	8.258	10.391
Theory (Ref. 13)	5.886	89.24	0.0217	50.96	8.268	10.329
Experiment (Ref. 12)	5.98	88.35	0.0248	53.31	8.334	10.651
Experiment (Ref. 33)	5.996	88.18	0.026	53.84	8.343	10.710

properties of GeTe. In Sec. IV, we present the calculated Born effective charge and optical dielectric tensors. In Secs. V and VI, the phonon band structure and infrared (IR) reflectivity are presented. In Secs. VII and VIII, we present the elastic and piezoelectric properties.

II. TECHNICAL INFORMATION

All the calculations have been performed using plane waves and norm-conserving pseudopotentials as implemented in the ABINIT code.[21,22] The dielectric, dynamical, elastic, and piezoelectric properties have been evaluated within the density functional perturbation theory.[23–26] We employed Hartwigsen-Goedecker-Hutter (HGH) pseudopotentials,[27] generated including spin-orbit coupling, within the local-density approximation adopting the Teter Pade parametrization.[28] Although this approximation is of frequent use and gives correct trends for the study of dielectric materials, one should be aware of some inherent limitations due to neglecting of the polarization dependence present in the "exact" functional.[29,30] The inclusion of spin-orbit coupling does not lead to noticeable changes for most of the results presented here, except for the electronic band structure, which was already known.[31] Even though HGH pseudopotentials are known for being relatively hard, the properties investigated in this work are well converged when including plane-wave basis up to a kinetic-energy cutoff equal to 15 Ha. The Brillouin-zone integration was performed using special k points sampled within the Monkhorst-Pack scheme.[32] We found that a mesh of $24\times24\times24$ k points was required to describe well the dielectric and vibrational properties. This k-point mesh guarantees a violation of charge neutrality less than $0.009e$. Such a low value is a good indicator of the adequate convergence of the calculations.

III. STRUCTURAL AND ELECTRONIC PROPERTIES

The ground-state rhombohedral structure of GeTe (space group $R3m$) has been represented in our calculations, taking the z axis along the [111] of the conventional distorted rocksalt structure with primitive translation vectors $(\frac{a}{4},-\frac{a}{4\sqrt{3}},\frac{c}{3})$, $(0,\frac{a}{2\sqrt{3}},\frac{c}{3})$, and $(-\frac{a}{4},-\frac{a}{4\sqrt{3}},\frac{c}{3})$, where the present a and c are related to a_0 and α in Table I via the relations $a=2a_0\sin(\frac{\alpha}{2})$ and $c=a_0\sqrt{3[1+2\cos(\alpha)]}$. In Table I, we report the calculated structural parameters. The lattice parameters (a_0), the angle (α), and the shift of the Ge and Te sublattices are reported using the distorted rocksalt setting: atomic positions are Ge (000) and ($0.5\text{-}\tau\,0.5\text{-}\tau\,0.5\text{-}\tau$) for Ge and Te, respectively. Our results are globally in good agreement with previously reported *ab initio* results.[13] Moreover the deviation between the calculated structural parameters (a_0,α) and experiment is less than 2%.

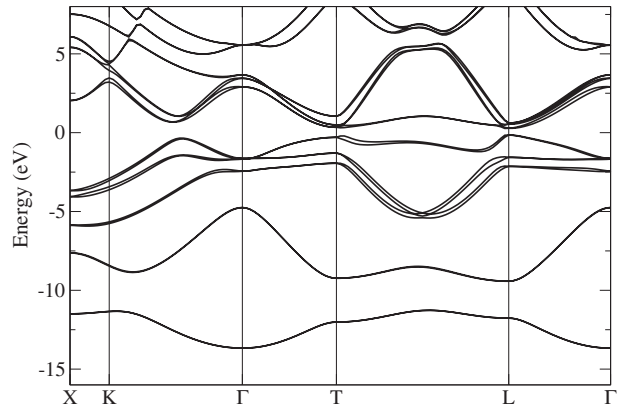

FIG. 1. Calculated band structure of rhombohedral GeTe. The top of valence band is set to zero.

In Fig. 1 we show the energy-band structure calculated using the theoretical structural parameters from Table I. The general features of the band structure agree with previously reported *ab initio* calculations.[7,13] The calculated direct energy gap at L is 0.48 eV; this value is slightly larger than the previously reported *ab initio* results of 0.40 (Ref. 7) and 0.369 eV.[13] The indirect gap that exists at L (0.35,0.2,0.2) is 0.28 eV, which is slightly bigger than the tunneling spectroscopy results, 0.2 eV.[34] Since the electronic gap is quite sensitive to the distortions, it was suggested by Rabe and Joannopoulos[7] that such overestimation of the gap can be due to the difference between the theoretical structural parameters used in the calculations and those of the thin films used in the tunneling spectroscopy measurements.

IV. DIELECTRIC PROPERTIES

We have first calculated the Born effective charge tensor of atom κ, which is defined as the induced polarization of the solid along the direction i by a unit displacement in the direction j of the sublattice of atom κ at vanishing electric field E,

$$Z^*_{\kappa,ij}=\Omega\left.\frac{\partial P_i}{\partial a_{\kappa j}}\right|_{E=0}. \quad (1)$$

Using Eq. (1), the Born effective charge tensor can be calculated using DFPT or within the finite-difference method (FDM). In the latter case the polarization is calculated using the Berry phase technique.[35] We have employed both methods in this study, and the results are shown in Tables II and III. In Table II we demonstrate the convergence of Born effective charge with respect to the cut-off energy and k-point

TABLE II. Components of the Born effective charge tensor of Ge and Te calculated by DFPT.

		Ge		Te	
k-point mesh	Cutoff	$Z^*_\perp$	$Z^*_\parallel$	$Z^*_\perp$	$Z^*_\parallel$
$12\times12\times12$	15	6.771	4.550	−6.638	−4.479
$12\times12\times12$	20	6.772	4.547	−6.638	−4.477
$16\times16\times16$	15	6.834	4.596	−6.780	−4.560
$20\times20\times20$	15	6.872	4.589	−6.850	−4.573
$24\times24\times24$	15	6.889	4.580	−6.881	−4.573
$28\times28\times28$	15	6.897	4.574	−6.894	−4.571

grids. Table II shows that Z^* components change at most by $\leq 0.003e$ as the cut-off energy increases from 15 to 20 hartree, on the other hand, a $24\times24\times24$ k-point mesh was necessary to get well-converged results and reduce the violation of charge neutrality below $0.009e$.

Due to the symmetry properties of $R3m$ structure, the Born effective charge tensors of Ge and Te are diagonal, with two independent components, along ($Z^*_\parallel$) and perpendicular ($Z^*_\perp$) to the trigonal axis. The Born effective charge tensor is strongly anisotropic with a difference of 2.2 between $Z^*_\parallel$ and $Z^*_\perp$ components. Both $Z^*_\perp$ and $Z^*_\parallel$ are significantly larger than the nominal ionic value of +2 for Ge and −2 for Te.[36] This is a consequence of partial hybridization of the p orbitals of both Ge and Te which results in a mixed ionic-covalent bond.

Our results for the Born effective charge of the ferroelectric phase differ widely from the previous results obtained using the Berry phase and FDM.[13] A value of $Z^*_\parallel = 10.11$ was reported which is much larger than our calculated value of 4.58. However, the agreement between Z^* from DFPT and Z^* from FDM, as clearly seen in Table III, questions the accuracy of the results obtained in Ref. 13.

The values of both $Z^*_\parallel$ and $Z^*_\perp$ are also smaller than those theoretically obtained for rocksalt high-temperature phase.[8,15] It has been noted previously that for perovskite systems, Z^* is strongly dependent on the geometry.[16] To get more insight about the evolution of Z^* due to the paraelectric-ferroelectric phase transition, we have evaluated Z^* as a function of atomic distortions. Starting from the paraelectric cubic phase, we manually displaced atoms with small steps to their theoretically optimized positions in the rhombohedral symmetry, calculating Z^* at each step. The calculations were done by keeping the unit-cell structure fixed at the high-temperature cubic lattice parameters. The results are plotted in Fig. 2(a). At $\lambda=0$, the atoms occupy the high-symmetry sites as required by high-temperature paraelectric

TABLE III. Components of the Born effective charge tensor of Ge as calculated by DFPT and FDM. We show also the calculated optical dielectric tensor in units of vacuum permittivity ε_0.

DFPT		FDM			
$Z^*_\perp$	$Z^*_\parallel$	$Z^*_\perp$	$Z^*_\parallel$	$\varepsilon^\infty_\perp$	$\varepsilon^\infty_\parallel$
6.89	4.58	6.90	4.49	60.78	49.95

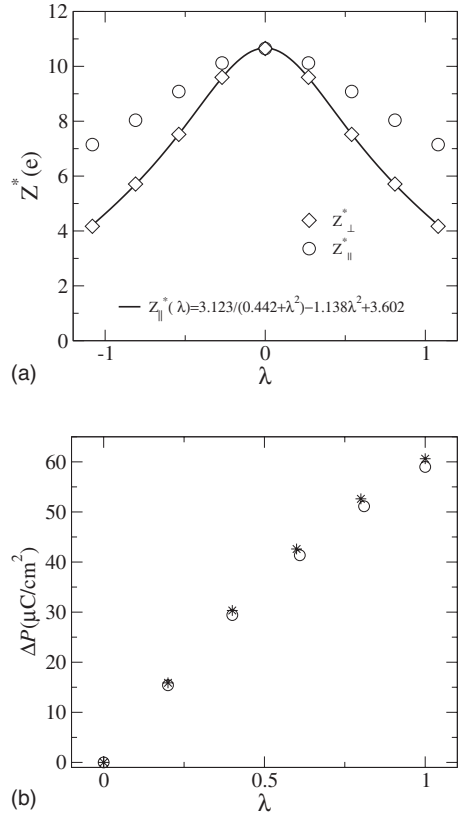

FIG. 2. (a) Evolution of Born effective charge tensor components along the path of atomic displacement from the cubic $\lambda=0$ to the rhombohedral $\lambda=+1$ (or -1) phase. The distortion of the unit cell has been neglected. (b) The polarization difference evaluated using the Berry phase technique as a function of λ at fixed cubic unit cell (circle) and fixed rhombohedral unit cell (star).

phase, while at $\lambda=1,-1$ the atoms occupy the theoretically optimized positions in the rhombohedral symmetry along $\langle 111\rangle$ and $\langle \bar{1}\bar{1}\bar{1}\rangle$, respectively. As seen in Fig. 2(a), the Born effective charge in the rocksalt phase is 10.68, which is in good agreement with the theoretical results of Waghmare *et al.*,[15] who reported a value of 10.8. It has been shown previously that such high value of Born effective charge can be due to the extremely narrow electronic gap possessed by the high-temperature rocksalt phase.[8] We have noticed that both $Z^*_\perp$ and $Z^*_\parallel$ drop as the atoms approach the ferroelectric sites. Such modification of charge with atomic position is considered a feature similar to what was obtained previously in the case of ABO_3 perovskites.[37]

The Born effective charge evolution can be used to estimate the spontaneous polarization. The polarization difference ΔP along a direction i is evaluated as the sum of the products of the atomic displacements and the corresponding Born effective charges,

$$\delta P_i = \frac{e}{\Omega}\sum_{\kappa,j} Z^\star_{\kappa,ij}\delta u_{\kappa,j}, \tag{2}$$

where $\delta u_{\kappa,j}$ is the atomic displacement of atom κ in the direction of Cartesian direction j. Integrating the polarization

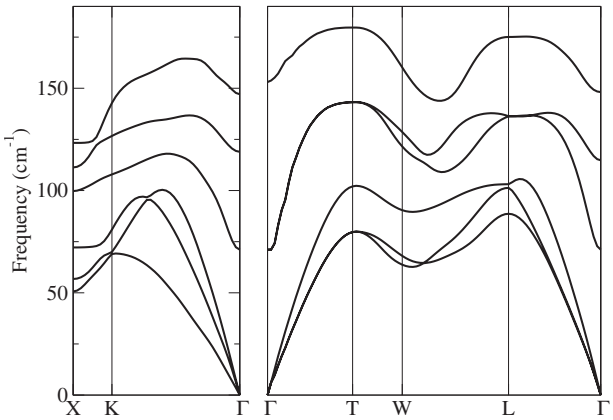

FIG. 3. Calculated phonon-dispersion curves of ferroelectric GeTe at the theoretical lattice parameters.

change along the path connecting the two end points, $\lambda=0$ (paraelectric) and 1 (ferroelectric), gives

$$\Delta P_i = \frac{e}{\Omega}\sum_{\kappa,j}\Delta u_{\kappa,j}\int_0^1 Z^{\star}_{\kappa,ij}(\lambda)d\lambda. \quad (3)$$

Using the above equation, we evaluated ΔP along the z direction (ΔP_3) using the fitted curve of $Z^*_{\parallel}$ given in Fig. 2(a) and found a value of $\Delta P_3=60\ \mu\mathrm{C/m}^2$. On the other hand ΔP_i can be calculated by taking the difference between $P(\lambda=0)$ and $P(\lambda)$ using the Berry phase technique. In Fig. 2(b), we show the Berry phase results of ΔP that are calculated at several points along the path from $\lambda=0$ to $\lambda=1$. To apply such a technique, one has to work at fixed unit-cell shape and size. As seen in Fig. 2(b), we did not find a noticeable difference if the calculations are made considering either the fixed rhombohedral or cubic unit cell (only the internal atomic coordinates vary). In agreement with the results obtained by using Eq. (3), the polarization difference between the two end points is $\sim 60\ \mu\mathrm{C/m}^2$.

Similar to the effective charge tensor, the calculated dielectric tensors are diagonal consisting of two independent components, which are parallel and perpendicular to the trigonal axis. Our value is larger than the previously reported experimental value (35–37.5).[38] Generally speaking, the high value of (ε^{∞}) comes as a consequence of the low value of the electronic gap.

V. DYNAMICAL PROPERTIES

Since there are two atoms per primitive unit cell, there will be six phonon branches. The phonon branches are divided into three acoustic and three optical phonon modes. Along the Γ-T direction (trigonal axis), the phonon-dispersion curves can be classified as E or A_1 according to whether the atomic displacements are perpendicular or parallel to the trigonal axis, respectively. Along the other directions, the branches cannot be classified as pure E or A_1 modes.

In Fig. 3, we show the calculated phonon band structure obtained by DFPT. The general features of the band structure are close to those of Bi which has a similar structural unit cell.[39] Because of the nonvanishing components of the Born effective charge tensors, the dipole-dipole interaction had to be properly included in the calculation of the interatomic force constants.[25] Such inclusion of the dipole-dipole interaction in the interatomic force constants results in splitting of longitudinal optic (LO) and transverse optic modes (LO-TO splitting). Within this treatment, the A_1 and E modes (for wave vector aligned with the trigonal direction) are characterized as LO and TO modes, respectively. With the crystal being uniaxial, the LO-TO splitting at Γ might vary with the limiting direction. We actually noticed a very strong dependence of the LO-TO splitting on the wave vector.

TABLE IV. Phonon frequencies at the zone center (in cm^{-1}) calculated for a **q** vector parallel to trigonal axis.

	E (TO)	A_1 (LO)
Semiconducting	73	152
Complete screening	73	121
Experiment (Ref. 4)	98	140
Experiment (Ref. 5)	80	122

It is difficult to grow large high-quality GeTe crystals, so little experimental information on its vibrational modes has been collected. The comparison between the calculated mode frequencies at Γ and those measured by Raman-scattering experiments is also difficult.[4,5] It is quite known that GeTe samples are nonstoichiometric and contain a high concentration of free holes.[40] This results in a complete screening of the dipole-dipole interaction by the conduction electrons at the zone center.[4] However, the comparison can be possible if we artificially enforce such a complete screening of the dipole-dipole interaction at the zone center. This can be achieved by simply eliminating the nonanalytical contribution of the long-range dipole-dipole interaction at Γ. The results are shown in Table IV: the first row contains the values of frequencies as calculated by including the dipole-dipole interaction using a semiconducting screening and the second row contains the values of frequency as calculated by complete screening of the dipole-dipole interaction.[41] We note that the values calculated by complete screening of the long-range force are in more agreement with the recent Raman inelastic-scattering results.[5] Note that in the absence of the LO-TO splitting, as a result of complete screening of dipole-dipole interaction, the A_1 mode has been characterized experimentally as a TO mode. In fact, it was suggested that the softening of this mode at the critical temperature is responsible for the ferroelectric-paraelectric transition.[4,41]

VI. INFRARED SPECTROSCOPY

The dielectric tensor $\varepsilon(\omega)$ in the lowest frequency range can be related experimentally to the IR spectra. It can be calculated theoretically by accounting for ionic relaxations in the calculations of the permittivity tensor. The ionic contribution to $\varepsilon(\omega)$ comes mainly from optical phonon contributions (without damping) to the IR oscillator strength $S_{m,ij}$,

TABLE V. Calculated values of IR oscillator strength tensor $S(1\times10^{-5})$ (in atomic unit) of optical modes and components of static permittivity tensor in units of ε_0.

	$\perp$	$\parallel$
$S(E)$	56.20	0.00
$S(A_1)$	0.00	24.83
$\varepsilon(0)$	247.32	68.67

$$\varepsilon_{ij}(\omega) = \varepsilon_{ij}^{\infty} + \frac{4\pi}{\Omega}\sum_{m}^{\mathrm{TO}} \frac{S_{m,ij}}{\omega_m^2 - \omega^2}, \tag{4}$$

where Ω is the volume of unit cell and m is the phonon mode rank.

In Table V, we present the calculated IR oscillator strength and the components of $\varepsilon(0)$ for a perfect semiconductor GeTe crystal. From Table V, it is obvious that the ionic contribution to $\varepsilon(0)_\perp$ comes purely from E modes and to $\varepsilon(0)_\parallel$ from A_1 mode. The inclusion of the ionic contribution results in a strongly anisotropic $\varepsilon(0)$ with $\varepsilon(0)_\perp$, which is almost three times larger than $\varepsilon(0)_\parallel$. In fact, the strong anisotropy of $\varepsilon(0)$ has been expected in regard of the frequency difference between $E(73\ \mathrm{cm}^{-1})$ and $A_1(121\ \mathrm{cm}^{-1})$ modes. Another reason for the large anisotropy comes from the fact that one $S_\perp$ of E modes is almost twice $S_\parallel$ of A_1 mode.

In Fig. 4 we present the calculated IR reflectivity associated with E and A_1 modes. The reflectivity related to A_1 mode can be associated with light incident parallel to the trigonal axis of the crystal, i.e., perpendicular to (001) surface. Similarly, the E modes reflectivity shall be associated with light incident perpendicular to the trigonal axis, i.e., parallel to a (b) directions which are perpendicular to 100 (010) surfaces.

The range of light wavelength at which the maximum reflectivity occurs differs depending on the surface. For example, whereas the maximum reflectivity for light incident on (001) surface occurs for wavelengths in the range 65–83 μm, it is in the range 68–137 μm in case of 100 or 010 surfaces.

VII. ELASTIC PROPERTIES

In this section we present our results for the elastic and compliance tensors. The elastic tensor is defined as the

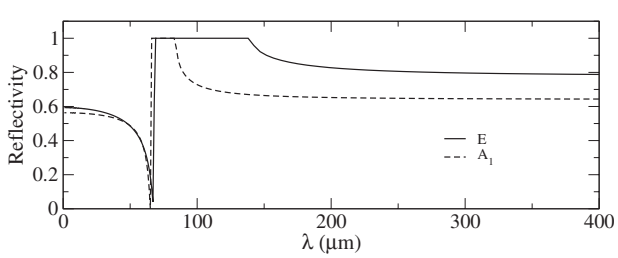

FIG. 4. Calculated IR reflectivity spectra of GeTe (without anharmonic damping).

TABLE VI. Clamped ion c^0 and relaxed ion c elastic tensors (GPa), and clamped ion s^0 and relaxed ion s compliance tensors (in TPa^{-1}).

Index	c^0	c	s^0	s
11	115.70	112.00	11.73	12.32
12	22.41	19.36	−2.38	−2.92
13	36.76	27.20	−3.97	−4.29
14	27.04	24.40	−5.86	−8.45
33	86.51	59.51	14.93	20.72
44	65.05	44.02	20.25	32.07

change in the stress of the solid in the direction α as the strain changes in the direction β, where $\alpha,\beta=1\ldots6$ in Voigt notation,

$$c_{\alpha\beta} = \frac{\partial\sigma_\alpha}{\partial\eta_\beta}. \tag{5}$$

The above equation splits into two main contributions

$$c_{\alpha\beta} = \left.\frac{\partial\sigma_\alpha}{\partial\eta_\beta}\right|_u + \sum_k \frac{\partial\sigma_\sigma}{\partial u_{k,i}}\frac{\partial u_{k,i}}{\partial\eta_\beta}. \tag{6}$$

The first term is the frozen (clamped) ion elastic tensor (c^0) and the second term includes contributions from force-response internal stress and displacement-response internal strain tensors. The second term accounts for the ionic relaxations in response to strain perturbations. The addition of the two contributions is the relaxed ion elastic tensor c. The compliance tensor is simply defined as the inverse of the elastic tensor.

In Table VI, we show our results for the elastic and compliance tensors. Due to the low symmetry of $R3m$ of rhombohedral phase of GeTe, there are six independent elastic constants. The obtained values for the elastic tensor constants satisfy the mechanical stability restrictions for trigonal-like unit cells $c_{11}-|c_{12}|>0$, $(c_{11}+c_{12})c_{13}-2c_{13}^2>0$, and $(c_{11}-c_{12})c_{44}-2c_{14}^2>0$.[42] Usually, the inclusion of internal relaxations reduces the values of elastic tensor components due to the relief of stress tensor components. The same behavior is also reflected in the increase in the compliance tensor components. The effect of internal relaxation is more pronounced in the case of c_{33} which represents the axial shear along the surface perpendicular to the threefold rotation axis. However, one should emphasize here that the effect of internal atomic relaxation is not as strong as for other materials such as ZnO and $BaTiO_3$.[26] The small differences between the clamped and relaxed compliance tensors might explain the similarity of the bulk modulus of the ferroelectric and the rocksalt phases, as has been suggested by the experimental findings.[12]

The bulk modulus can be readily calculated, using the above results, from the compliance tensor[43]

TABLE VII. Independent components of proper homogeneous piezoelectric tensor e^0, internal strain piezoelectric tensor, and proper total piezoelectric tensor (in C/m^2). The piezoelectric constant tensor d (in pC/N) and the electromechanical coupling constants k are also given.

	15	21	31	33
e^0	0.90	1.27	0.92	−0.29
Internal strain	−5.89	−0.73	−0.95	−2.67
Total	−4.99	0.53	−0.03	−2.96
d	−169.02	50.21	12.46	−61.17
k	0.54	0.26	0.13	0.48

$$B = \left[\sum_{\alpha\beta}^{3} s_{\alpha\beta} \right]^{-1}. \tag{7}$$

Using the above equation, we get a value of $B=44.80$ GPa which is in quite good agreement with the experimental value of 49.96 ± 3.2 GPa.[12]

We have also calculated the bulk modulus by fitting the total energy as a function of volume curve using the Murnaghan equation of state. The obtained value of $B=44.3$ GPa is in much better agreement with experimental findings than the theoretical value reported in Ref. 13.

Unfortunately we are not aware of any experimental result for the elastic constants of GeTe. The agreement between the value of the bulk modulus value extracted from the elastic tensor and those calculated by fitting to the equation of state or measured in experiment nevertheless insures the overall reliability of the calculated values of the elastic tensor.

VIII. PIEZOELECTRIC PROPERTIES

The proper piezoelectric tensor e is defined as the induced polarization in i direction due to a strain change for index α,

$$e_{i\alpha} = \frac{\partial P_i'}{\partial \eta_\alpha} \tag{8}$$

$$= \left. \frac{\partial P_i'}{\partial \eta_\alpha} \right|_u + \sum_k \frac{\partial P_i'}{\partial u_{ik}} \frac{\partial u_{ik}}{\partial \eta_\alpha}, \tag{9}$$

where P_i' is the reduced (rescaled) polarization as defined in the Appendix of Ref. 26. The first term is the proper homogeneous strain contribution to the piezoelectric tensor e^0 which arises mainly from the sole electronic contribution. The second term, often called internal strain piezoelectric tensor, includes contributions from the Born effective charge tensor diagonal and internal relaxation. The second term represents the ionic contribution to piezoelectric tensor.

In Table VII, we present the results for the piezoelectric tensor. There are four independent components. The components e_{31} and e_{33} represent the induced polarization along the trigonal axis created in response to shear strain in the ab plane and along the trigonal axis, respectively. The other components describe the induced polarization along the primitive axes (a,b) by shear strain. The calculated value of e_{33} is -2.96 (C/m^2). The proper homogeneous strain contribution was found to be -0.29 (C/m^2); however, the strain contribution is much larger, adding -2.67 (C/m^2). The strain contribution was relatively large in the case of e_{15} with a value of -5.89 (C/m^2). The strain contribution of the last case being twice the value of e_{33} can be explained by the noticeable anisotropy in the Born effective charge and by the large strain-induced ionic motion in the lateral direction in response of a strain applied along the trigonal axis. For the other elements, the strain contribution reduces the polarization, which is almost cancelled, as in the case of e_{31}.

The efficiency of the produced electric energy vs the spent mechanical energy can be estimated by calculating the electromechanical coupling constant, which is defined as

$$k_{i\alpha} = \frac{|d_{i\alpha}|}{\sqrt{\varepsilon_{ii}^{\sigma} S_{\alpha\alpha}}}, \tag{10}$$

where $d_{i\alpha}$ is the piezoelectric constant, $d_{i\alpha}=S_{\alpha\beta}e_{i\beta}$, and ε^σ is the free stress dielectric tensor related to the vanishing strain dielectric tensor shown in Table VII via Eq. 20 of Ref. 26.

Similar to the zero strain dielectric tensor ε, the stress-free dielectric tensor ε^σ is diagonal with two independent values $\varepsilon_{\parallel}^{\sigma}=89.06\varepsilon^0$ and $\varepsilon_{\perp}^{\sigma}=348.60\varepsilon^0$. Note that ε^σ have components larger than ε as expected for any piezoelectric material.

In the last two rows of Table VII, we show our calculated piezoelectric constants d and electromechanical coupling constants. Even though the various components of d are quite smaller than those reported for $0.71Pb(Mg_{1/3}Nb_{2/3})O_3$-$0.29(PbTiO_3)$ system,[44] it is interesting that our calculated value of d_{15} is comparable with that of the giant piezoelectric materials $0.58Pb(Mg_{1/3}Nb_{2/3})O_3$-$0.42(PbTiO_3)$ (Ref. 45) where d_{15} extends between 131 and 190 pC/N. On the other hand, the calculated electromechanical coupling factors, in general, are far less compared with that of PMN-PT (Ref. 45) or PMNT (Ref. 44); however, they are slightly better than those of ZnO.[26]

IX. CONCLUSION

We have investigated the dielectric, dynamical, and mechanical properties of the ferroelectric phase of GeTe within density functional perturbation theory. Our study covers all the linear couplings among applied static homogeneous electric field, strain, and periodic atomic displacements: Born effective charge, dynamical matrix at the zone center, clamped and dressed elastic constants, optical dielectric tensor, adiabatic dielectric tensor, free stress dielectric tensor, piezoelectric coefficients, and elastic and compliance tensors. We also examined the phonon band structure as well as the change of the Born effective charge tensor with the atomic positions. Our other results have also been discussed and compared with the available theoretical and experimental results.

ACKNOWLEDGMENTS

We acknowledge financial support from the Interuniversity Attraction Poles Program (Grant No. P6/42)—Belgian

State—Belgian Science Policy. Two of the authors (R.S. and X.G.) acknowledge support from the Communaute Francaise de Belgique (Action de Recherches Concertee, Grant No. 07/12-003) and the European Union (Grant No. NMP4-CT-2004-500198) ("NANOQUANTA" Network of Excellence "Nanoscale Quantum Simulations for Nanostructures and Advanced Materials" and "ETSF" Integrated Infrastructure Initiative) and FAME-EMMI Network of Excellence "Functionalized Advanced Materials Engineering." We would also like to thank Manuel Cardona for a critical reading of the paper.

[1] S. Ovshinsky, Phys. Rev. Lett. **21**, 1450 (1968).
[2] M. Libera and M. Chen, J. Appl. Phys. **73**, 2272 (1993).
[3] N. Yamada, MRS Bull. **21**, 48 (1996).
[4] E. F. Steigmeier and G. Harbeke, Solid State Commun. **8**, 1275 (1970).
[5] K. Andrikopoulos, S. Yannopoulos, G. Voyiatzis, A. Kolobov, M. Ribes, and J. Tominaga, J. Phys.: Condens. Matter **18**, 965 (2006).
[6] J. Y. Raty, V. V. Godlevsky, J. P. Gaspard, C. Bichara, M. Bionducci, R. Bellissent, R. Céolin, J. R. Chelikowsky, and P. Ghosez, Phys. Rev. B **65**, 115205 (2002).
[7] K. M. Rabe and J. D. Joannopoulos, Phys. Rev. B **36**, 6631 (1987).
[8] N. E. Zein, V. I. Zinenko, and A. S. Fedorov, Phys. Lett. A **164**, 115 (1992).
[9] P. B. Littlewood, J. Phys. C **13**, 4875 (1980).
[10] T. Chattopadhyay, J. X. Boucherle, and H. G. von Schnering, J. Phys. C **20**, 1431 (1987).
[11] A. I. Lebedev, I. A. Sluchinskaya, V. N. Demin, and I. H. Munro, Phys. Rev. B **55**, 14770 (1997).
[12] A. Onodera, I. Sakamoto, Y. Fujii, N. Môri, and S. Sugai, Phys. Rev. B **56**, 7935 (1997).
[13] A. Ciucivara, B. R. Sahu, and L. Kleinman, Phys. Rev. B **73**, 214105 (2006).
[14] K. M. Rabe and J. D. Joannopoulos, Phys. Rev. Lett. **59**, 570 (1987).
[15] U. V. Waghmare, N. A. Spaldin, H. C. Kandpal, and Ram Seshadri, Phys. Rev. B **67**, 125111 (2003).
[16] Ph. Ghosez, X. Gonze, Ph. Lambin, and J.-P. Michenaud, Phys. Rev. B **51**, 6765 (1995).
[17] Xuhui Sun, Bin Yu, Garrick Ng, and M. Meyyappan, J. Phys. Chem. C **111**, 2421 (2007).
[18] Se-Ho Lee, Dong-Kyun Ko, Yeonwoong Jung, and Ritesh Agarwal, Appl. Phys. Lett. **89**, 223116 (2006).
[19] S. Prosandeev, I. Ponomareva, I. Kornev, I. Naumov, and L. Bellaiche, Phys. Rev. Lett. **96**, 237601 (2006).
[20] I. Naumov, L. Bellaiche, and H. Fu, Nature (London) **432**, 737 (2004).
[21] X. Gonze, J.-M. Beuken, R. Caracas, F. Detraux, M. Fuchs, G.-M. Rignanese, L. Sindic, M. Verstraete, G. Zerah, F. Jollet, M. Torrent, A. Roy, M. Mikami, Ph. Ghosez, J.-Y. Raty, and D. C. Allan, Comput. Mater. Sci. **25**, 478 (2002).
[22] X. Gonze, G.-M. Rignanese, M. Verstraete, J.-M. Beuken, Y. Pouillon, R. Caracas, F. Jollet, M. Torrent, G. Zerah, M. Mikami, P. Ghosez, M. Veithen, J. Y. Raty, V. Olevano, F. Bruneval, L. Reining, R. Godby, G. Onida, D. R. Hamann, and D. C. Allan, Z. Kristallogr. **220**, 558 (2005).
[23] For a review, S. Baroni, S. de Gironcoli, A. Dal Corso, and P. Giannozzi, Rev. Mod. Phys. **73**, 515 (2001).
[24] X. Gonze, Phys. Rev. B **55**, 10337 (1997).
[25] X. Gonze and C. Lee, Phys. Rev. B **55**, 10355 (1997).
[26] Xifan Wu, D. Vanderbilt, and D. R. Hamann, Phys. Rev. B **72**, 035105 (2005).
[27] C. Hartwigsen, S. Goedecker, and J. Hutter, Phys. Rev. B **58**, 3641 (1998).
[28] S. Goedecker, M. Teter, and J. Hutter, Phys. Rev. B **54**, 1703 (1996).
[29] X. Gonze, P. Ghosez, and R. W. Godby, Phys. Rev. Lett. **74**, 4035 (1995).
[30] X. Gonze, P. Ghosez, and R. W. Godby, Phys. Rev. Lett. **78**, 294 (1997).
[31] Y. W. Tung and M. L. Cohen, Phys. Rev. **180**, 823 (1969).
[32] H. J. Monkhorst and J. D. Pack, Phys. Rev. B **13**, 5188 (1976).
[33] J. C. S. Goldak, D. I. Barrett, and W. Youdelis, J. Chem. Phys. **44**, 3323 (1966).
[34] L. L. Chang, P. J. Stiles, and L. Esaki, IBM J. Res. Dev. **10**, 484 (1966).
[35] D. Vanderbilt and R. D. King-Smith, Phys. Rev. B **48**, 4442 (1993).
[36] The nominal ionic value of Ge in tetrahedral covalent crystals is +4. However in binary compounds as IV-VI, it is considered +2 which is the negative of the nominal ionic value of Te.
[37] Ph. Ghosez, J.-P. Michenaud, and X. Gonze, Phys. Rev. B **58**, 6224 (1998).
[38] R. Tsu, W. Howard, and L. Esaki, Phys. Rev. **172**, 779 (1968).
[39] L. E. Diaz-Sanchez, A. H. Romero, and X. Gonze, Phys. Rev. B **76**, 104302 (2007).
[40] S. Bahl and K. Chopra, J. Appl. Phys. **41**, 2196 (1970).
[41] In practice, the screening of the depolarizing field associated with the A1(LO) mode will reduce its frequency to that of A1(TO) mode.
[42] M. Born and K. Huang, *Dynamical Theory of Crystal Lattices* (Oxford University Press, London, 1954).
[43] J. F. Nye, *Physical Properties of Crystals: Their Representation by Tensors and Matrices* (Oxford University Press, New York, 1985).
[44] F. Wang, L. Luo, D. Zhou, X. Zhao, and Haosu Luo, Appl. Phys. Lett. **90**, 212903 (2007).
[45] Hu Cao, V. Hugo Schmidt, Rui Zhang, Wenwu Cao, and Haosu Luo, J. Appl. Phys. **96**, 549 (2004).